Optimization of intrinsic self-healing silicone coatings by benzotriazole loaded mesoporous silica

Chen, Guangmeng; Wen, Shifeng; Ma, Jiacheng; Sun, Zhiyong; Lin, Cunguo; Yue, Zhufeng; Mol, J. M.C.; Liu, Ming

DOI
10.1016/j.surfcoat.2021.127388

Publication date
2021

Document Version
Final published version

Published in
Surface and Coatings Technology

Citation (APA)
Chen, G., Wen, S., Ma, J., Sun, Z., Lin, C., Yue, Z., Mol, J. M. C., & Liu, M. (2021). Optimization of intrinsic self-healing silicone coatings by benzotriazole loaded mesoporous silica. *Surface and Coatings Technology*, *421*, Article 127388. https://doi.org/10.1016/j.surfcoat.2021.127388

Surface & Coatings Technology 421 (2021) 127388

Contents lists available at ScienceDirect

Surface & Coatings Technology

journal homepage: www.elsevier.com/locate/surfcoat

Optimization of intrinsic self-healing silicone coatings by benzotriazole loaded mesoporous silica

Guangmeng Chen [a], Shifeng Wen [a,*], Jiacheng Ma [a], Zhiyong Sun [b], Cunguo Lin [b], Zhufeng Yue [a], J.M.C. Mol [c], Ming Liu [c,d]

[a] School of Mechanics and Civil & Architecture, Northwestern Polytechnical University, Xi'an, 710129, PR China
[b] State Key Laboratory for Marine Corrosion and Protection, Luoyang Ship Material Research Institute, Qingdao 266101, PR China
[c] Department of Materials Science and Engineering, Delft University of Technology, Delft, the Netherlands
[d] State Key Laboratory for Strength and Vibration of Mechanical Structures, Xi'an Jiaotong University, Xi'an 710049, PR China

ARTICLE INFO

Keywords:
Self-healing coating
BTA leaching
Corrosion protection
Urea hydrogen
Mechanical strength

ABSTRACT

Multifunctional intrinsic self-healing polymers (ISP) are gaining increasing attention these days, and many studies have been devoted to solving the conflict between achieving high mechanical polymer strength and active polymer chain diffusion. In this research, we developed an optimized self-healing composite coating by adding Benzotriazole (BTA) loaded nano silica (SiO_2@BTA) to a dynamic cross-linked Polydimethylsiloxane (PDMS) network , which allows substantial and fast healing of the material integrity upon damage due to the hydrogen interaction between urea and BTA. BTA leaching tests demonstrated a longer release profile during the coating service life and corrosion tests in a 3.5 wt% NaCl aqueous solution indicated that the SiO_2@BTA modified PDMS coating shows enhanced corrosion protection of carbon steel upon coating damage. Moreover, after addition of SiO_2@BTA, the material failure strength increased from ~1.5 MPa to ~5.5 MPa, and the healing efficiency increased from ~59% to ~90% for 24 h healing at room temperature. Above all, this research provides an intrinsic self-healing coating design method to improve the mechanical strength and the self-healing ability of the ISP as well as enhancing the coating's corrosion protection ability.

1. Introduction

Inspired by self-healing concepts present in the natural world, intrinsic self-healing polymers cross-linked by dynamic reversible bonds have gained a lot of research interest because of their promising application in flexible electronics [1], adhesives [2–3], biomedicines [4–7], protective coatings [8–9], and other areas of technological interest [10]. Considering their self-restoring property upon damage, intrinsic self-healing polymers are ideal materials for corrosion protective coatings by autonomous recovery of barrier protection [11]. To date, the study of intrinsic self-healing polymer in corrosion protective coating has been relatively limited, which from a technological point of view can be attributed to some important barriers inherent to the self-healing concepts so far.

Firstly, some typical coating materials used for corrosion protective coatings, such as epoxies and polyurethanes, usually need high cross-linking density to prevent corrosive medium diffusion, i.e. providing barrier protection, which on the other hand intrinsically hampers the self-healing process requiring active polymer chain diffusion [12–14]. Furthermore, it generally takes several to dozens of hours after the occurrence of coating damage to complete the self-healing process at room temperature [15–16]. This delayed self-healing action may provide a protection issue, as corrosion may start off as soon as the metal substrates are exposed to a corrosive medium. As a result, substantial corrosion may occur before the repairing of the scratch, indicating the importance of optimized inhibitor and healing agent release and coating matrix self-repair kinetics. Also, the self-healing ability of the scratch is restricted by the extent of damage, for example coating scratch defect width, because the self-healing process depends on the filling of neighboring material through polymer chain diffusion and dynamic exchanging reaction. Therefore, when the scratch size is much larger than the coating thickness, the scratch could not be repaired to its full extent because there is not sufficient material to fill the crack.

Except for intrinsic self-healing, there is another self-healing strategy, namely extrinsic self-healing, which relies on self-healing action by adding corrosion inhibitors to the coating to prevent excessive corrosion

* Corresponding author.
E-mail address: wenshifeng@nwpu.edu.cn (S. Wen).

https://doi.org/10.1016/j.surfcoat.2021.127388
Received 2 March 2021; Received in revised form 1 June 2021; Accepted 2 June 2021
Available online 7 June 2021

in coating defects [17–20]. To prevent inhibitor-coating matrix interaction and optimizing the leaching kinetics of protective compounds such as corrosion inhibitors, smart leaching concepts are introduced into the coating matrix by adding delivery systems such as micro- or nano-containers loaded with active inhibitive pigments [9,21–24] or organic compounds [11,25]. Nano silica, a readily available ceramic, was most widely used as nano-container material to load inhibitors due to its simple preparation method, high specific surface area and flexible nano/micro structure [26–30]. Benzotriazole (BTA) and its derivatives have been unambiguously proven to be efficient for copper corrosion inhibition for the past few decades [31–34]. Furthermore, it has been shown to provide efficient protection to carbon steel and it is recognized that the dissolved BTA in water can form complex with Fe^{2+} that will deposit at a coating defect and block the water diffusion [35–36]. For example, Hao *et al.* used polyaniline decorated graphene as container material to load BTA and prepared a self-healing epoxy coating showing noticeably improved corrosion protection of carbon steel [36]. Except for its enhanced self-healing performance in corrosion protection, it is hard for extrinsic self-healing materials to achieve substantial healing of the material integrity upon damage due to irreversible cross-linking of typically used matrix material. Hence, it is a promising strategy to disperse inhibitor loaded nanocontainers within intrinsic self-healing matrix materials to provide coatings with high-effective self-healing properties.

In addition, a key challenge remains in solving the conflict between mechanical strength and self-healing ability for intrinsic self-healing. More specifically, high mechanical strength indicates high cross-linking density which limits polymer chain diffusion while active chain diffusion is essential for reversible association-disassociation reactions of the dynamic cross-linking points. In recent years, significant efforts have been made into high performance self-healing materials. One of the most effective methods is to combine two or more types of reversible bonds in one self-healing system to enable a hierarchical energy dissipation mechanism [14,37]. In addition, other researchers also put forward the method of designing multiphase self-assembly of supramolecular structures to form a hard-soft microphase-separated system [12,38–39]. For example, in the extant literature, You et al. reported a highly efficient self-healing elastomer (Cu–DOU–CPU) with synergistic triple dynamic bonds [40–41]. Experiments showed that the mechanical strength and self-healing ability can be simultaneously improved by the coordination of Cu(II). Density functional theory calculations also revealed the critical role of Cu(II) in accelerating the reversible dissociation of dimethylglyoxime–urethane. A dynamic self-healing PDMS (polydimethylsiloxane) material cross-linked by reversible urea hydrogen bonds and imine bonds (UI) was studied in our previous work [42–43]. The dynamic network consists of urea hard segments and imine soft segments. Changing the urea-to-imine ratio, an optimized self-healing material was obtained with urea-to-imine ratio at 1:1, which exhibits significant self-healing and corrosion protection. However, the improvement of mechanical strength was restricted because of the intrinsic conflict between mechanical strength and self-healing property, which restricts its practical application, to date.

In order to improve intrinsic self-healing, corrosion protective properties in conjunction with enhanced mechanical strength, we have developed an optimized intrinsic self-healing composite coating by dispersing inhibitor 1H-Benzotriazole (BTA)-loaded mesoporous nano silica (SiO_2@BTA) into a dynamic UI network. The reversible cross-linked PDMS matrix achieved substantial and fast healing of the material integrity upon damage due to the hydrogen interaction between urea and BTA, which provides carbon steel with enhanced corrosion protection coating. At the same time, both the self-healing efficiency and the mechanical properties of the UI dynamic network could be improved simultaneously by the incorporation of SiO_2@BTA. It is promising to form a self-healing material development strategy to minimize the commonly observed intrinsic conflict between high mechanical polymer strength and active polymer chain diffusion.

2. Experimental section

2.1. Base chemicals

Aminopropyl terminated polydimethylsiloxane (AP-PDMS, type KF-8010) was purchased from Shin-Etsu. Isophthalaldehyde (IPAL) and 4,4′-methylenebis-(cyclohexyl isocyanate) (HMDI) were purchased from Macklin and Sigma, respectively. 1H-Benzotriazole (BTA) and hexadecyl trimethyl ammonium bromide (CTAB) were provided by Aladdin. Ethyl alcohol, tetrahydrofuran (THF), tetraethyl orthosilicate (TEOS), and triethanolamine (TEA) were purchased from Sinopharm Chemical Reagent Co., Ltd. THF was dehydrated with molecular sieves before use and other reagents were used as received.

2.2. Preparation of UI

UI was synthesized according to our previous reported method with modification [43]. In this study, we used PDMS with a molecular weight of 860 g/mol to obtain a stronger material. To synthesize self-healing PDMS-based material, PDMS (0.01 mol) and THF (100 mL) were added to a 250 mL three-necked round-bottom flask which was equipped with reflux device and purged by dry N_2. When the system was heated to 60 °C in an oil bath under a N_2 atmosphere, HMDI (0.005 mol) was poured dropwise into the mixture to react throughout vigorous stirring for 6 h. Subsequently, IPAL (0.005 mol) was added and stirred for another 6 h at 60 °C. The bubbles of the resulting liquid mixture were removed using a vacuum pump. Finally, the self-healing material was obtained by pouring the mixture into a Teflon casting dish and dried at room temperature for 3 days to evaporate the solvent. The synthetic procedure and chemical structure of UI were shown in Scheme 1.

2.3. Preparation of SiO_2@BTA

The nanosilica was synthesized applying the procedure introduced by Borisova et al. [44]. In this work, CTAB was used as template and other aspects of the procedure were unchanged. After the reaction, the silica was separated by centrifugation and then washed with ethyl alcohol two times to remove the unreacted reagents. Finally, the mesoporous nanosilica was obtained after calcination at 600 °C for 8 h to remove the template completely. To prepare SiO_2@BTA, 10 mg/mL water solution of the mesoporous nanosilica was mixed with aqueous 1H-benzotriazole (BTA) solution (10 mg/mL) at a volume ratio of 1:1, then the mixture was vacuumized and stirred at room temperature for 2 h. After that, the loaded silica was separated by centrifugation and then dried overnight in a vacuum oven at 60 °C.

2.4. Preparation of UIB-x ($x = 1 \sim 4$)

The preparation process of self-healing materials is shown in Scheme 2. The materials with SiO_2@BTA concentrations in UI matrix of 1.3 wt%, 2.5 wt%, 5 wt% and 7.5 wt% were named as UIB-1, UIB-2, UIB-3, UIB-4, respectively. To disperse SiO_2@BTA into the UI network, 16 g of UI was dissolved in 60 mL THF. SiO_2@BTA was dispersed in 20 mL THF and then treated by sonication at room temperature for 10 min. Then the dispersion was mixed with the UI solution and stirred at room temperature for 2 h. The bubbles of the resulting liquid mixture were removed using a vacuum pump. Finally, the self-healing materials were obtained by pouring the mixture into a Teflon casting dish and dried at room temperature for 3 days to evaporate the solvent. The material with only 5 wt% of pure SiO_2 was prepared as unactivated contrast sample and named UIS. In addition, 0.1 g pure BTA is directly added to the UI solution to produce another control sample which was named UIB-0. For further guidance, the mass of components added in each sample is shown in Table 1.

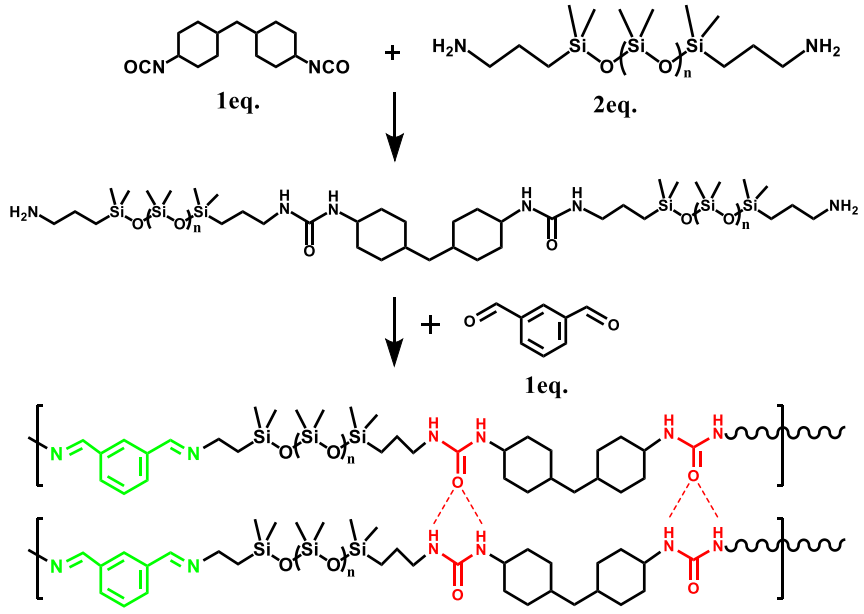

Scheme 1. Synthetic procedure and chemical structure of UI.

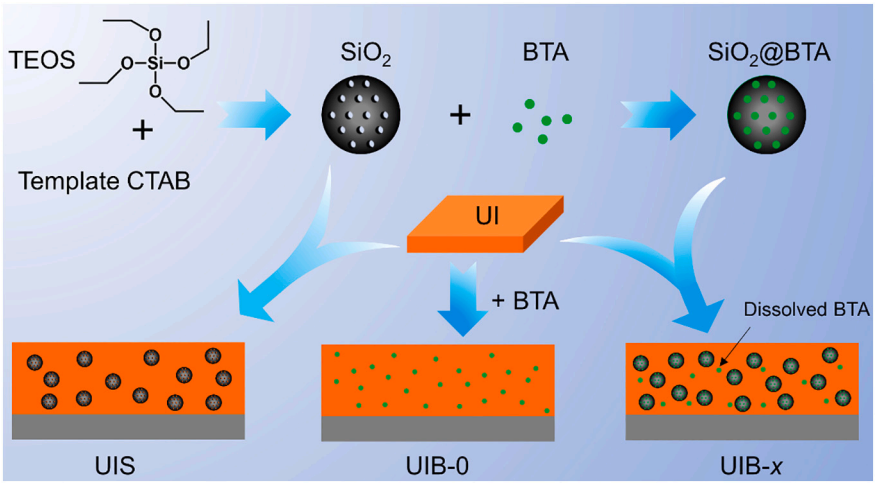

Scheme 2. Schematic of the experimental processes of UIS, UIB-0 and UIB-x (x = 1–4) coatings.

Table 1
The mass of each component added during preparation of UI, UIB-x (x = 0–4) and UIS.

Sample	The mass of each component added (g)				SiO_2@BTA concentration (wt%)
	UI	SiO_2@BTA	SiO_2	BTA	
UI	16	0	0	0	0
UIB-1	16	0.2	0	0	1.3
UIB-2	16	0.4	0	0	2.5
UIB-3	16	0.8	0	0	5
UIB-4	16	1.2	0	0	7.5
UIS	16	0	0.8	0	0
UIB-0	16	0	0	0.1	0

2.5. Characterization method

Scanning electron microscopy (Zeiss Gemini LEO1550) was employed to analyze silica samples at an operating voltage of 3 kV and working distance of 3 mm. The electron micrographs taken at different magnifications were obtained using backscattered electron imaging. Fourier Transform Infrared (FT-IR) spectra were recorded on an iS10 FTIR spectrometer with a resolution of 2 cm^{-1} and with the accumulation of 32 scans. The silica powder samples were analyzed using the KBr disk method and the film samples were studied using the attenuated total reflection unit. N_2 adsorption/desorption measurements were performed on the system Micromeritics TriStar 3000 to study the porosity of the samples. Optical images were obtained with an optical microscopy VHX-5000 instrument. The UV–Vis absorption spectra were tested using ultraviolet–visible absorption spectrometry (UV–vis N4S). To study the BTA release behavior, a piece of material with dimensions of 1 mm × 1.5 mm × 1.5 mm was immersed in 50 mL ultrapure water. The UV–vis absorption spectra were obtained at discrete exposure times during an overall exposure time of 250 h. The DSC and TG tests were characterized by using a Q200 thermogravimetric analyzer (TA Instruments). The temperature range tested was from 25 °C to 800 °C with a heat rate of 10 °C min^{-1} in nitrogen atmosphere. N_2 adsorption/desorption measurements at 77 K were performed on the system Micromeritics ASAP 2460 to study the porosity of the samples. These were pretreated by outgassing under vacuum at 423 K. The pore size

distributions were obtained by applying the BET and BJH model isotherms. Particle size distributions of SiO_2 and SiO_2@BTA were tested by Dynamic Light Scattering (DLS) method. The Nano laser particle size distribution analyzer JL-1198 was purchased from Chengdu Jingxin Powder Testing Equipment Co., Ltd.. Before testing, SiO_2 and SiO2@BTA were dispersed in water by ultrasonic treatment for 15 min respectively to get uniform transparent solution. Then we use the transmission method to test the size distribution. Every sample was tested for three times to minimize random error. DSC measurement was performed on a TA DSC214 differential scanning calorimeter from Netzsch at the heating rate of 10 °C min^{-1}. XRD measurements was performed on Shimadzu XRD-7000 under Cu Kα radiation (λ =0.1541 nm). XRD spectra from 3° to 60° were obtained at a speed of 5° min^{-1}.

Mechanical tensile-stress tests were carried out with an INSTRON 3366 tensile testing machine at room temperature at a speed of 50 mm/min. The samples were cut into dumbbell shape with dimensions of 5 mm (width) × 1 mm (thickness), the gauge length was 20 mm. To test the self-healing property, the dumbbell samples were cut into two pieces, then the cut surfaces were put in contact by hands and then put at room temperature to heal for scheduled time. The stress-strain curves were measured after healing for 6 h, 12 h and up to 24 h. Every test was repeated at least three times to validate reproducibility of the measurements. The self-healing efficiency is defined as the ratio of maximum strain between the healed and initial sample. The stress relaxation studies were conducted by inducing a constant initial strain (ε = 100%) of the gel sample in stretch mode at room temperature. The relaxation modulus G(t) was normalized by initial value G(0).

To test the corrosion performance of coated substrates, the prepared dry material was dissolved in THF (1 g in 10 mL THF), then 200 μL of the solution was coated on the surface of Q235 carbon steel with a surface area of 1.5 × 1.5 cm. Finally, the sample was used after drying for 7 days at room temperature in air. The dry thickness of coatings was measured to be approximately 100 μm using the digital thickness gauge QNix 4500. Electrochemical impedance spectroscopy (EIS) measurements of the coated steel samples were performed in a 3.5 wt% NaCl solution by using a three-electrode system, in which the coated steel serves as the working electrode, a saturated calomel electrode as the reference and a platinum electrode as the counter electrode. EIS measurements were performed with a CS350 electrochemical workstation at the open circuit potential (OCP). The applied frequency range was 10^{-2}–10^{5} Hz with a signal amplitude of 20 mV vs OCP. In addition, to test the corrosion protection ability in the presence of a scratch, the coatings were scratched vigorously with a scalpel to ensure the scratch cut through the coating into the steel substrate before immersion into 3.5 wt% NaCl solution.

3. Results and discussion

3.1. Preparation of BTA-loaded mesoporous nano SiO_2 (SiO_2@BTA)

Mesoporous SiO_2 nanoparticles were prepared by dehydration and condensation of ethyl orthosilicate with CTAB as template. The inhibitor BTA was loaded to the mesoporous SiO_2 in water. SEM results showed that the loading of BTA did not have obvious effect on the surface morphology of SiO_2 as shown in Fig. 1. The particle size distributions of SiO_2 and SiO2@BTA were tested by DLS, and the results were shown in Fig. S1. The average particle size of SiO_2 and SiO_2@BTA were 156.7 ± 2.5 nm and 164.8 ± 2 nm. Fig. 2 shows the characterization results of the mesoporous SiO_2 before and after loading. FTIR in Fig. 2(a) shows that after being loaded with BTA, a new peak appeared at 746 cm^{-1}, which is the 1,2–substitution in the benzene ring in the BTA structure [35]. TG analysis shown in Fig. 2(b) indicated a fast weight loss at 200–300 °C for SiO_2@BTA and a distinct absorbance peak was observed at 220 °C in the DSC curve due to the vaporization of BTA at this temperature [35]. The adsorption-desorption behavior of N_2 delivered a type-IV isotherm with two typical closed hysteresis loops as shown in Fig. 2(c), which indicates that the mesoporous structure of nanosilica was successfully prepared [44]. N_2 sorption measurements were performed to observe the change in nanoparticle porosity and reduction of total pore volume with BTA loading. As shown in Fig. 2(d) and Table 2, the average pore size decreased from 3.0 nm to 2.7 nm after loading of BTA. The surface area also decreased from 883.45 m^2/g to 693.32 m^2/g and the pore volume decreased significantly. The aforementioned results indicate that the loading of BTA filled the mesoporous structure of nanosilica. The loading efficiency can be estimated using N_2 sorption by computing the reduction in total pore volume.

3.2. Morphology characterization

Fig. 3 shows the surface SEM images of different coatings. Fig. 3(a) shows that the surface of coating UI is relatively smooth, indicating a pure polymer without any pigment. A few SiO_2 particles can be found on the surfaces of UIB-1, UIB-2 and UIB-3, which results from the relatively low concentration of SiO_2@BTA in it. When the SiO_2@BTA concentration increased to 7.5 wt%, many outcrops can be observed on the surface of UIB-4, which indicates the SiO_2@BTA agglomerates in the coating. The EDX of UIB-4 is shown in Fig. S2, which indicates that the outcrop shows a low carbon and high oxygen content compared to that of the flat area, demonstrating that the outcrop is SiO_2@BTA agglomerates. The cross section SEM images are shown in Fig. 4. Fig. 4(a) shows that the cross section of UI is very smooth without any pigment. Fig. 4(b)–(d) shows that the SiO_2@BTA pigment dispersed uniformly in the coatings of UI-1, UI-2 and UI-3 with low pigment concentrations. When the SiO_2@BAT concentration increased to 7.5 wt%, obvious SiO_2 agglomerates can be found in Fig. 4(e) and (f) for coating UIB-4. The EDX also

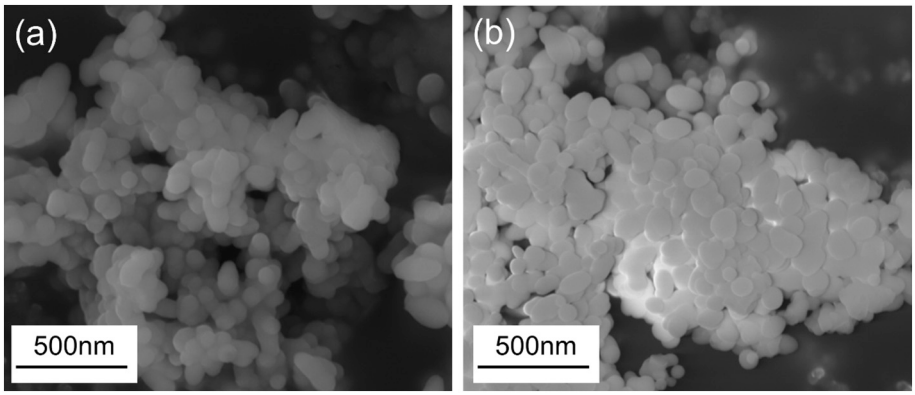

Fig. 1. SEM micrographs of SiO_2 (a) and SiO_2@BTA (b).

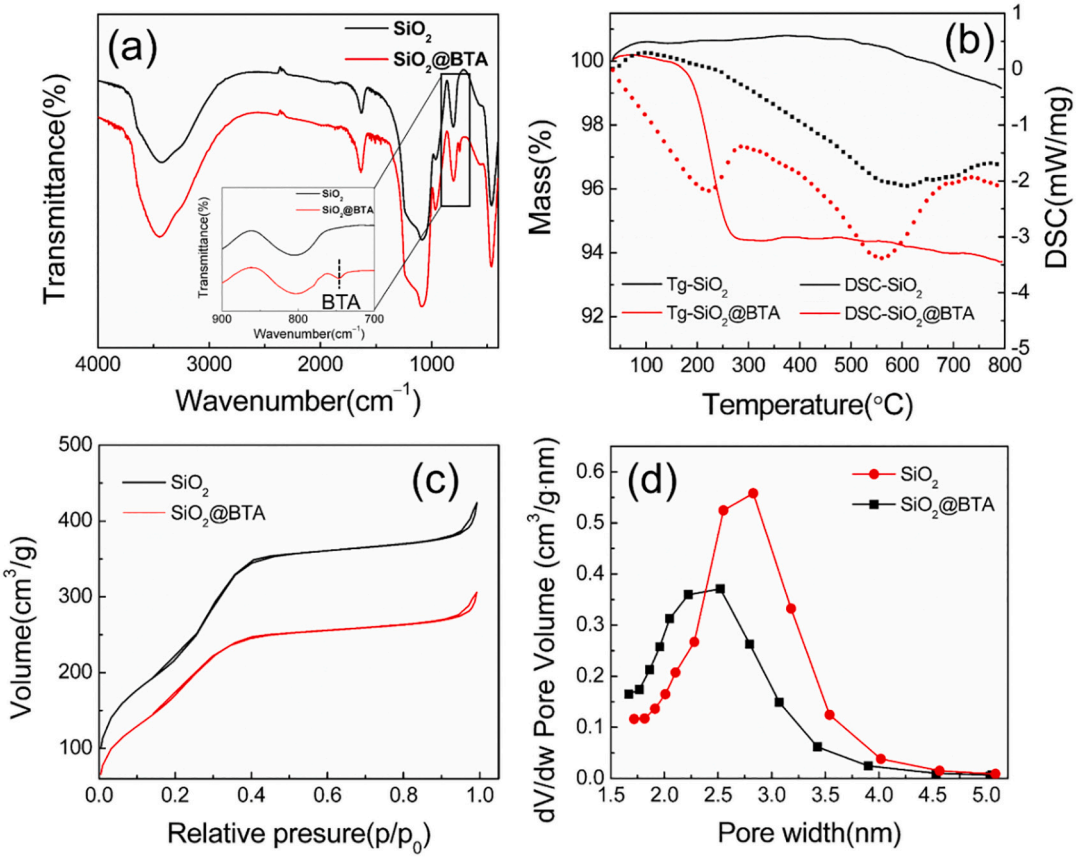

Fig. 2. Characterization of SiO_2 and SiO_2@BTA: (a) FTIR spectrum. (b) TG and DSC curves. (c) N_2 sorption isotherm. (d) Pore size distribution.

Table 2
N_2 sorption results of SiO_2 and BTA-loaded SiO_2 (SiO_2@BTA).

	Surface area(m^2/g)	Pore volume(cm^3/g)	Average diameter(nm)
SiO_2	883.45	0.66	2.97
SiO_2@BTA	693.32	0.47	2.73

demonstrated that the agglomerates is SiO_2 as shown in Fig. S3.

3.3. Mechanical properties

The mechanical properties of the differently prepared coatings were studied by uniaxial tensile testing at a loading speed of 50 mm/min and the results are shown in Fig. 5. When SiO_2@BTA is not added, i.e. for the sample UI, the coating exhibits a relatively poor mechanical strength with a failure stress of ~1.5 MPa. With an increase of the SiO_2@BTA content from 1.3% to 7.5%, the mechanical strength increased significantly from 2.7 ± 0.2 MPa to 7.9 ± 0.04 MPa, more than five times the original strength of the coating matrix. The elongation at failure

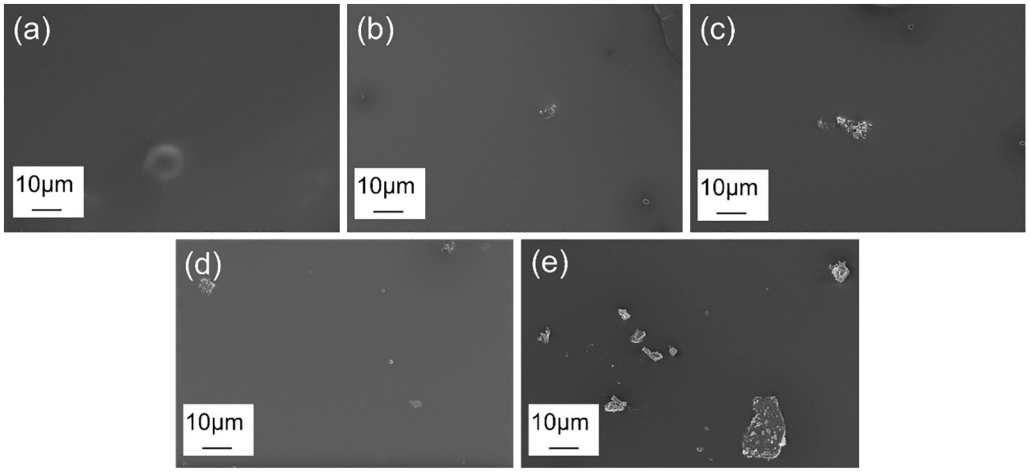

Fig. 3. The surface SEM images of different coatings, (a) UI, (b) UIB-1, (c) UIB-2, (d) UIB-3, (e) UIB-4.

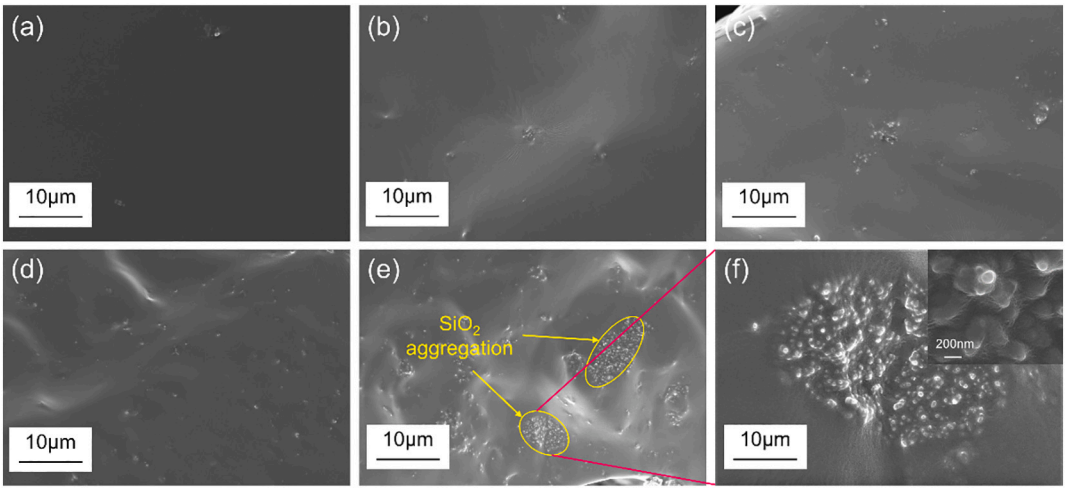

Fig. 4. The cross section SEM images of different coatings, (a) UI, (b) UIB-1, (c) UIB-2, (d) UIB-3, (e) UIB-4, (f) high magnification images of UIB-4.

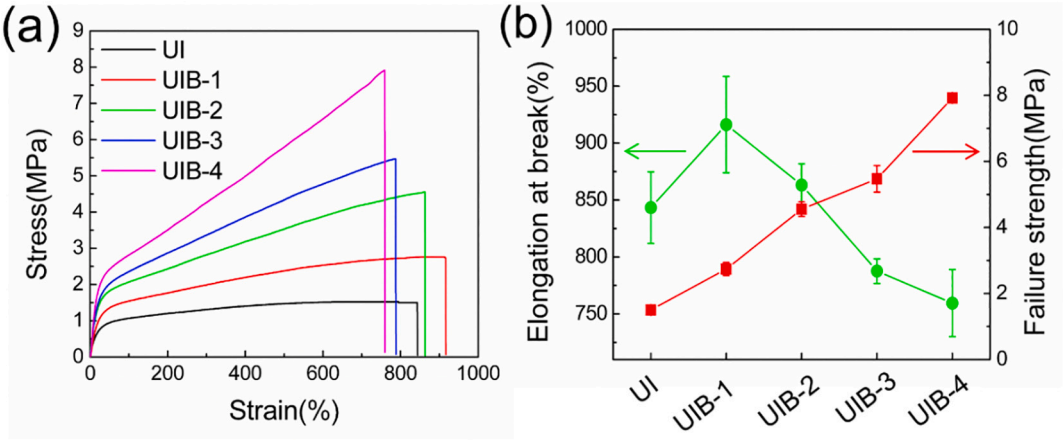

Fig. 5. (a) Stress-strain curves of self-healing materials with different contents of SiO_2@BTA. (b) Elongation at break and failure strength.

demonstrated an increase for the sample with a concentration of SiO_2@BTA of 1.3% as compared to that for the coating matrix, being approximately 916 ± 42% and 843 ± 32% respectively. It then decreased gradually with further addition of SiO_2@BTA to 759 ± 30% at a concentration of 7.5 wt% SiO_2@BTA. The change of mechanical behavior in terms of strength and ductility can be explained by the synergistic effect of the addition of nanosilica and BTA. The increase of mechanical strength resulted from the enhancement effect of silica nanoparticle, which mainly ascribes to two factors. Firstly, addition of silica particle increased the fraction of hard component, resulting in increase of the initial modulus and fracture strength. In the other hand, the cross-linking density was increased by reaction between hydroxyl in the surface of silica and UI network by hydrogen bonds. In addition, some PDMS chains were strongly absorbed at the particle surface, which formed macroscopic networks [45–47]. Meanwhile, when SiO_2@BTA was added into UI solution, the BTA dissolved in THF formed hydrogen bonds with the urea group of the coating matrix, which destroyed the hydrogen bonds structure between urea groups. In this way, it is beneficially accommodating the diffusion capacity of the UI polymer chain in hard segments. As a result, the ductility improved for UIB-1 with low concentration of SiO_2@BTA. However, when the concentration of silica particle is increased further, silica aggregation (shown in Fig. 4(e)) will restrict the chain diffusion, which offers an explanation to the decrease of ductility when the SiO_2@BTA concentration increases to more than 1.3%.

3.4. Self-healing properties

The self-healing properties of materials with different SiO_2@BTA concentration were studied by tensile testing and a scratch healing test. The stress-strain curves and healing efficiency after healing at room temperature for different times are shown in Fig. 6. The UI sample exhibited a relatively slow self-healing ability showing a healing efficiency of only 25 ± 3% after 6 h of healing at room temperature. Further extension of healing time to 24 h resulted in a healing efficiency of 59 ± 14% as shown in Fig. 6(a). The addition of SiO_2@BTA shows to be beneficial to the self-healing process as shown in Fig. 6(b)–(d). The healing efficiency after 24 h increased gradually from 76 ± 7% to 90 ± 8% with increasing concentration of SiO_2@BTA from 1.3 wt% to 5 wt%. The maximal healing efficiency was obtained at a SiO_2@BTA concentration of 5 wt% (sample UIB-3) for each duration of healing at room temperature. It can be seen from Fig. 6(d) and (f) that, the healing efficiency reached 67 ± 9% after only 6 h of healing, which was even higher than that for UI after 24 h. Further increasing SiO_2@BTA concentration to 7.5% resulted in a drastic deterioration of self-healing ability where the self-healing is only 41 ± 7% after 24 h of healing, as shown in Fig. 6(e) and (f), which is even lower than that for UI. These results indicated that the addition of SiO_2@BTA was beneficial to the polymer self-healing process at least up to a concentration of 5 wt%. When the concentration increases further, it will have a negative effect on the polymer self-healing efficiency.

A dedicated scratch test was adopted to further verify the self-healing

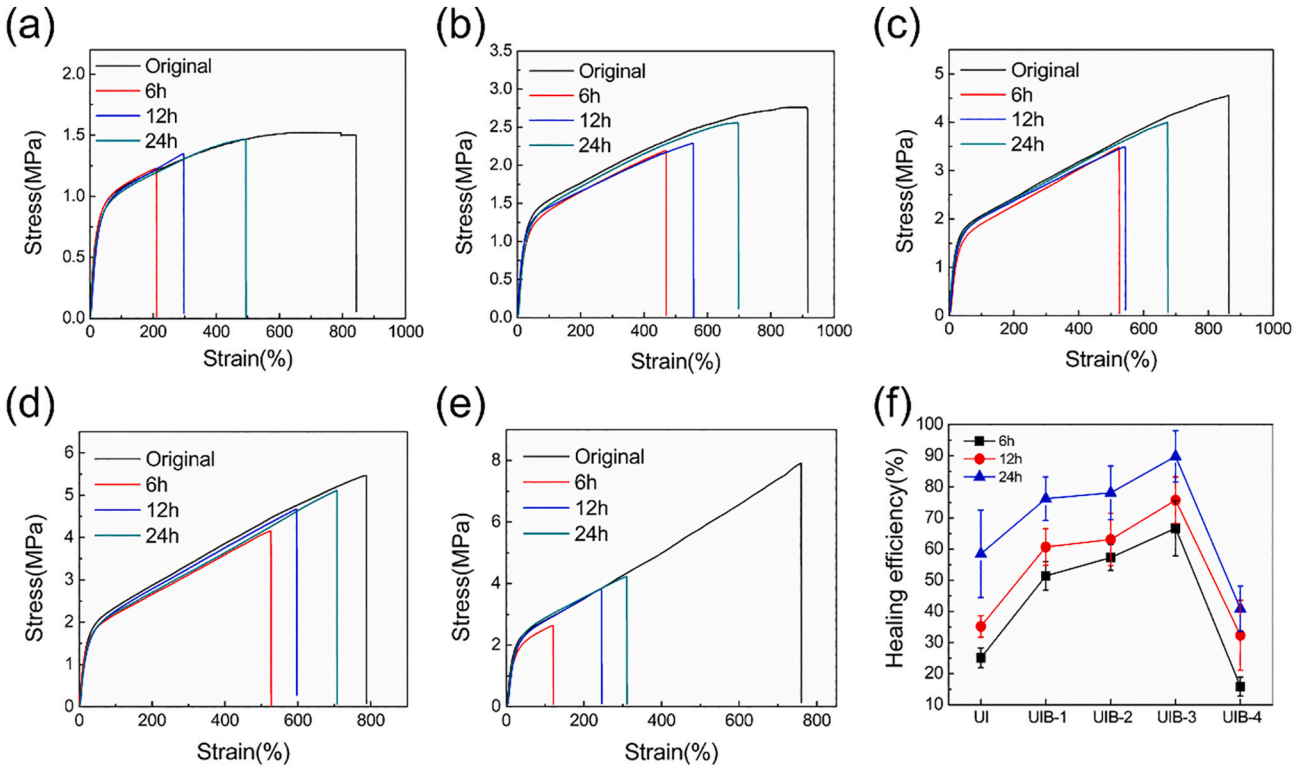

Fig. 6. Strain-stress curves of original and healed self-healing materials after different healing times at room temperature ((a)–(e): UI, UIB-1, UIB-2, UIB-3, UIB-4), the corresponding healing efficiency of the self-healing materials tested (f).

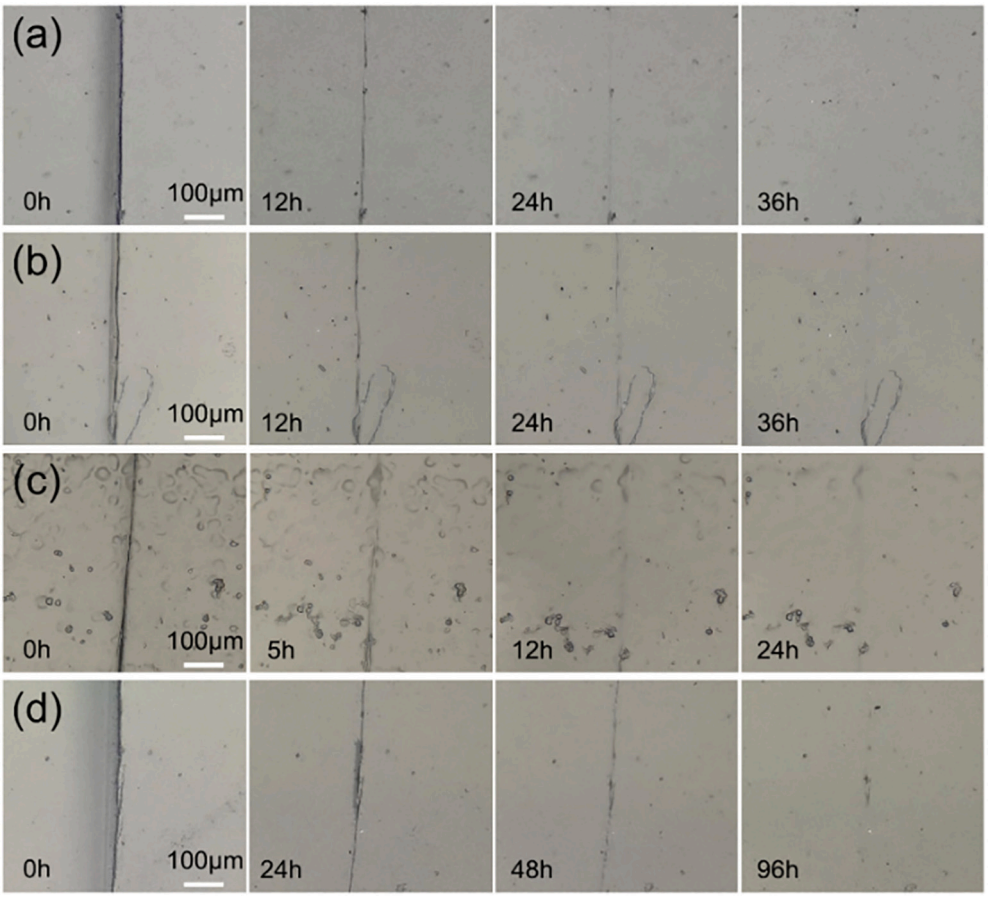

Fig. 7. Self-healing process of self-healing materials at room temperature with optical microscopic imaging ((a)–(d): UIB-1, UIB-2, UIB-3, UIB-4).

property of the materials tested. The scratch test of UI was studied in our previous study [43] and it took 72 h for the scratch to heal. As shown in Fig. 7, the addition of SiO_2@BTA leads to shorter times for scratch healing, which was 36 h for both UIB-1 and UIB-2. UIB-3 showed the shortest healing time, with the scratch healed within 24 h. When the concentration was increased to 7.5%, it exhibited a relatively long healing time of 96 h. These results further confirmed the self-healing ability tested by tensile testing. Based on the above results, it is shown that the BTA-silica container loading simultaneously improves the self-healing ability and mechanical strength of intrinsic self-healing UI materials.

3.5. The interaction between BTA and urea hydrogen

According to our previous studies [43], the self-healing property of UI was directly affected by the hydrogen bond density between urea groups and the reversible association-disassociation mechanism, as shown in Fig. S4. To study the variation of crystal density, DSC and XRD were applied and the results were shown in Fig. S8. It can be seen that no melt peak and crystal diffraction peak was found for UI, UIB-3 and UIB-0 (for these samples, the malar ratio of urea to imine is 1:1), which indicated that they are in the amorphous state at room temperature. To further study the crystallinity of urea group, we prepared the PDMS elastomer containing only urea group (marked as PU). The reaction procedure and chemical structure of PU was shown in Fig. S7. DSC result of PU showed a clear melt peak at 81.5 °C and RXD results also indicated the semi-crystalline property of PU [39]. We also found that PU exhibited poor self-healing property at room temperature as shown in Fig. S9. In conclusion, we find that urea group has crystalline property at room temperature, and becomes amorphous after combining urea and imine with molar ratio of 1:1.

We hypothesize that the improvement of the self-healing ability for the current modified UI matrix is caused by the decrease of hydrogen bonds density between urea groups due to the addition of BTA. More specifically, when SiO_2@BTA is added to UI solution, the exposed BTA molecule at the exterior surface of the nanosilica can form intermolecular hydrogen bonding with urea and the possible chemical structure is shown in Fig. 8(a). This may lead to a conclusion that the destruction of the regular structure of hydrogen bonds between urea decreased the energy barrier for the reversible association- dissociation reaction of urea hydrogen bonds and active originally inert hydrogen bonds in hard segments. However, the destruction of urea hydrogen bonds will also commonly cause the degeneration of mechanical strength because of the decrease cross-linking density. On the contrary, addition of nanoparticles is beneficial to the mechanical strength [48]. In consequence, the improvement of self-healing ability stems from the loading of BTA; the addition of silica nanoparticles account for the enhancement of mechanical strength. Therefore, the self-healing ability and mechanical strength can be improved simultaneously by increasing SiO_2@BTA concentration from 1.3 wt% to 5 wt%. By contrast, when the concentration of SiO_2@BTA increases to more than 5 wt%, silica nanoparticle aggregation may inhibit the chain diffusion, which negatively affects the polymer matrix self-healing property. This blocking effect may dominate the else beneficial effect of BTA. As a result, the self-healing ability improves with increased SiO_2@BTA content for relatively low concentrations of SiO_2@BTA and deteriorates markedly for higher levels of SiO_2@BTA with an optimal concentration at approximately 5 wt%.

To clarify the interaction between BTA and urea group, the FTIR spectrums of materials with different mass ratios of UI to BTA were mapped out. We mainly focus on the peak at around 3330 cm^{-1} and 1620–1650 cm^{-1}, which correspond to the N—H and C═O of the urea group respectively [49–50]. The full spectrum is shown in Fig. S5, and Fig. 8(b) shows the N—H stretching vibration peak in more detail. As the concentration of BTA increased from 1:0 to 4:1, the peak intensity of -NH at 3330 cm^{-1} decreased and shifted to 3359 cm^{-1}. Stretching vibration bands of urea carbonyl groups are shown in Fig. 8(c) where the peak at 1651 cm^{-1} corresponds to imine, and the peaks at 1628 cm^{-1} and 1644 cm^{-1} indicate the strong and weak urea hydrogen bonds respectively [50]. With the increase of BTA content, the peak at 1628 cm^{-1} diminished in intensity, the peak at 1644 cm^{-1} showed an apparently

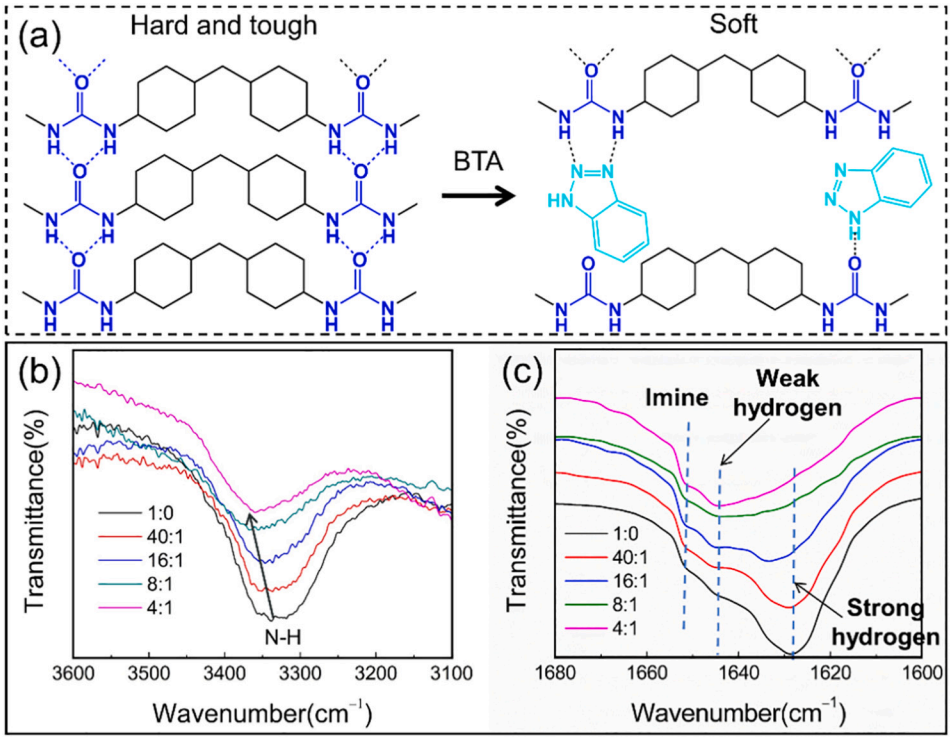

Fig. 8. (a) The schematic of hydrogen bonds between BTA molecule and urea group. (b) FTIR peak of N—H. (c) FTIR peak of imine and C═O with different hydrogen strength.

increasing trend and the imine peak at 1651 cm^{-1} remains unchanged. The FTIR peak transformations of N—H and C═O demonstrated the transformation from strong urea hydrogen to weak hydrogen bonds with increasing BTA concentration. The above results indicate that addition of BTA inhibits the formation of urea hydrogen bonds and decreases the hydrogen bond density of urea.

Two control materials UIS and UIB-0 were prepared to further verify the self-healing mechanism of the SiO_2@BTA enhanced self-healing materials. The self-healing results are shown in Fig. 9. Compared to UIB-3, UIS which was loaded with pure SiO_2 demonstrated higher mechanical strength with a failure strength up to 9.7 MPa (UIB-3 was 5.5 MPa) (Fig. 9(a)). However, as expected, UIS owned nearly no intrinsic self-healing ability reaching 16.7% after 24 hour healing at room temperature (being approximately 90% for UIB-3). The results indicate the strength reinforcement effect of SiO_2 and its negative effect on the self-healing process. By contrast, when we only added BTA to UI, the results were exactly the opposite. As shown in Fig. 9(b), the mechanical property deteriorated significantly upon adding BTA. The material demonstrated high ductility and the specimen did not fail upon stretching up to 2000% and the stress reduced to near-zero. Self-healing tests by uniaxial tensile testing of UIB-0 showed that the mechanical property can recover completely within 3 hour healing time at room temperature due to its high chain activity. Scratch tests indicated the same results as shown in Fig. 9(c) and (d). The scratch at the surface of UIS was difficult to heal even over a healing time of 10 days while the scratch of UIB-0 was completely healed within 3 h. These results further verify the effect of SiO_2 particle and BTA on the mechanical strength and self-healing property.

Stress relaxation tests were performed to evaluate the chain activity of the prepared self-healing materials and the results are shown in Fig. S6. The time required of each sample to relax to 1/e is defined as relaxation time (τ*) [37]. The τ* of UI was tested to be 77 s and that of UIS significantly higher, being 605 s. In comparison, the τ* of UIB-0 decreased to 19 s, which indicated the active diffusion of polymer chains. All these results have revealed the respective effects of SiO_2 capsules and BTA corrosion inhibitor on the mechanical and self-healing performance of the SiO_2@BTA enhanced self-healing elastomers.

3.6. Release of BTA

We monitored the BTA release process of the as-prepared self-healing materials by UV–vis absorption spectrum. The concentration−absorbance curve of BTA with different concentration levels in THF was used as a standard by measuring its absorbance at 259 nm where it shows the maximum absorbance value [51]. The absorbance spectra for different BTA concentration levels are shown in Fig. 10(a), and Fig. 10(b) presents the absorbance values at 259 nm. It can be seen that the concentration is proportional to the absorbance and the fitting curve and fitting equation are given in Fig. 10(b). The UV–vis absorption spectra of materials with different content of SiO_2@BTA tested at distinct times during 240 h are shown in Fig. S10. Fig. 10(c) shows the BTA concentration calculated using the standard fitting equation in Fig. 10(b). It was observed that the concentration increased exponentially with time. When considering the natural log of concentration (*lnC*) and time (*lnt*), it can be seen that *lnC* is proportional to *lnt* as shown in Fig. 10(d). In fact, the increase in inhibitor concentration in an electrolyte is often described by an exponential function of time [52–55]:

$C(t) = k\,t^n$, where $C(t)$ is the BTA concentration at time t; k is a constant incorporating initial conditions; n is the release exponent, indicative of the inhibitor release mechanism.

The dark lines in Fig. 10(d) give the fitting equation. The values of *lnk* and *n* are given in Table 3. The results indicate that all the materials

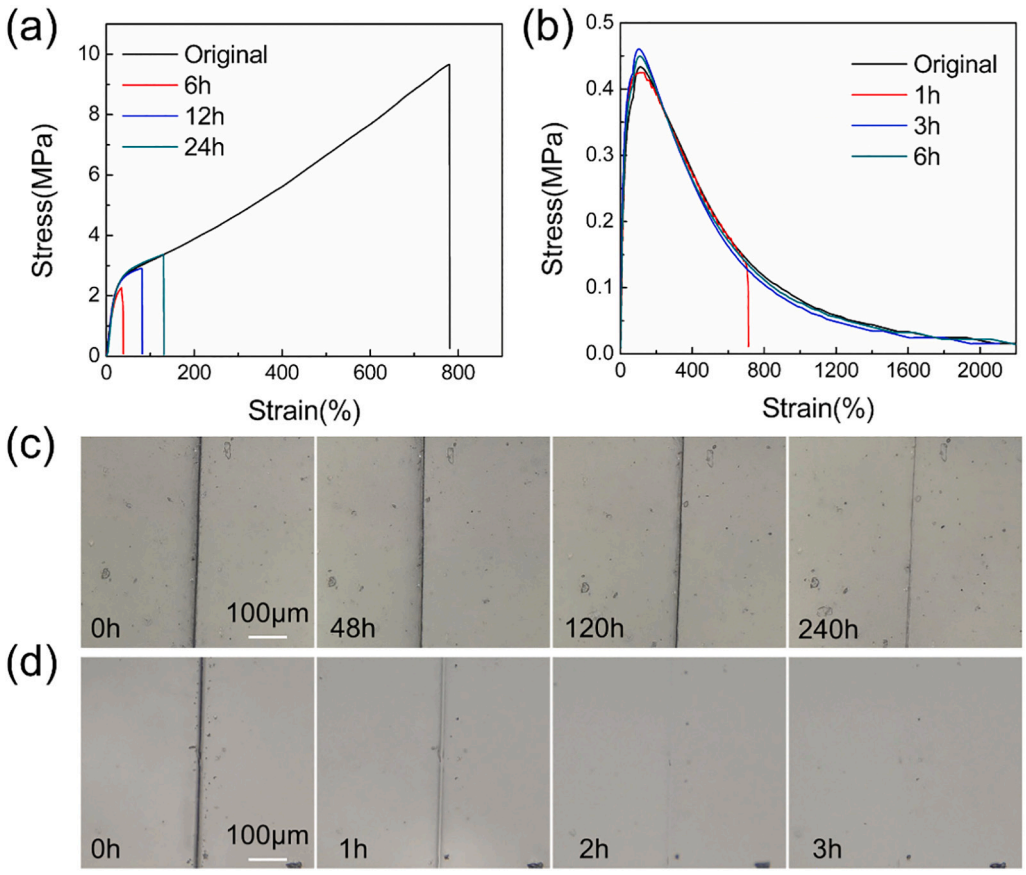

Fig. 9. Strain-stress curves of original and healed self-healing materials UIS (a) and UIB-0 (b) after different healing times at room temperature. Self-healing images of UIS (c) and UIB-0 (d) from an optical microscope at room temperature.

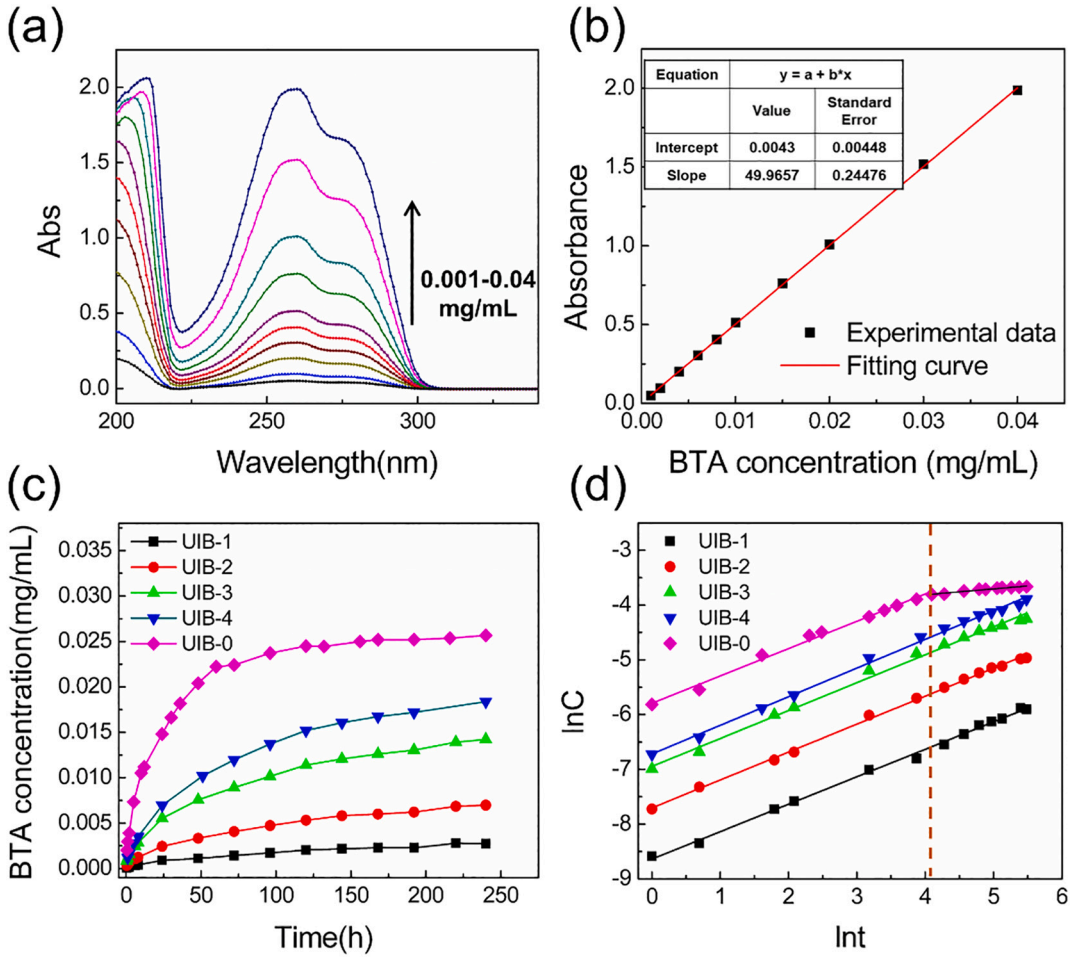

Fig. 10. (a) UV−vis absorption intensity of BTA aqueous solution with concentration levels from 0.001 to 0.04 mg/mL. (b) For the relationship between absorbance at 259 nm and BTA concentration, a fitting function was obtained as *"Concentration (mg/mL) = 49.97 × Absorbance + 0.0043"*. (c) BTA release curves of UIB-*x* (*x* = 0–4) in pure water. (d) The relationship between ln*C* and *lnt*. The points are experimental data and the dark lines indicate the fitting lines.

Table 3
The fitting values of *lnk* and *n* in the exponential model to describe the leaching process of BTA for coatings UIB-*x* (*x* = 0–4).

$C = k\,t^n$	*ln k*	*n*
UIB-1	−8.64	0.50
UIB-2	−7.70	0.51
UIB-3	−6.95	0.51
UIB-4	−6.72	0.52
UIB-0-1	−5.79	0.50
UIB-0-2	−4.24	0.11

own the same release exponent *n* of around 0.5, which means the release process is controlled by Fickian diffusion [56]. In addition, we can also see that *k* increased with SiO_2@BTA pigment concentration, due to the variation in initial concentration of BTA in the materials. For UIB-0, there was a critical point at 60 h, after which the BTA release did not follow this model and the BTA concentration hardly increases with time, which indicate BTA was used up and leaching process reached equilibrium. Other materials with SiO_2@BTA did not reach this critical point until 240 h, which revealed that SiO_2 can delay the BTA release possibly allowing a slower but longer release profile during the coating service life. We conjectured that there are three possible sources of the released BTA: (i) After BTA was loaded to silica, some BTA molecules was adsorbed on the outer surface of silica and dispersed in THF. The BTA dissolved in THF were not fully bonded to urea groups, the free BTA released to water during the soaking process; (ii) The materials swelled in water and the BAT in the mesoporous of silica dissolved in water and released gradually; (iii) There are several studies stated that the urea groups can interact with water molecule by hydrogen bonds [39], so it is possible that the BTA bonded to urea was replaced by water and released during soaking.

We also studied the mechanical properties of UIB-0 after being immersed in water. All of the tested samples were immersed in water for a specific period of time ranging from 0 to 10 days, and taken out to dry at room temperature for 5 days. The stress-strain curves are shown in Fig. S11. We found that the mechanical strength increased with immersion time during the first three days. This further confirmed the effect mechanism of BTA on the coating's mechanical property as discussed in Section 3.4. When the samples were immersed for more than three days, a possibly minor but non-significant change was observed regarding its mechanical strength, which was consistent with the critical point of about 60 h in the release curves in Fig. 10(d) showing a significant decrease in leaching rate from then onwards.

3.7. Corrosion protection performance

Finally, we studied the materials' corrosion protective property in an aqueous 3.5 wt% NaCl electrolyte. Before testing, we prepared the scratched coatings with scratch width of approximately 5 μm as measured in Fig. S12. Fig. 11 shows the EIS measurements of three coating-steel systems at different immersion times. As shown in Fig. 11 (a) and (b), the impedance modulus of UI coating system fall of over time

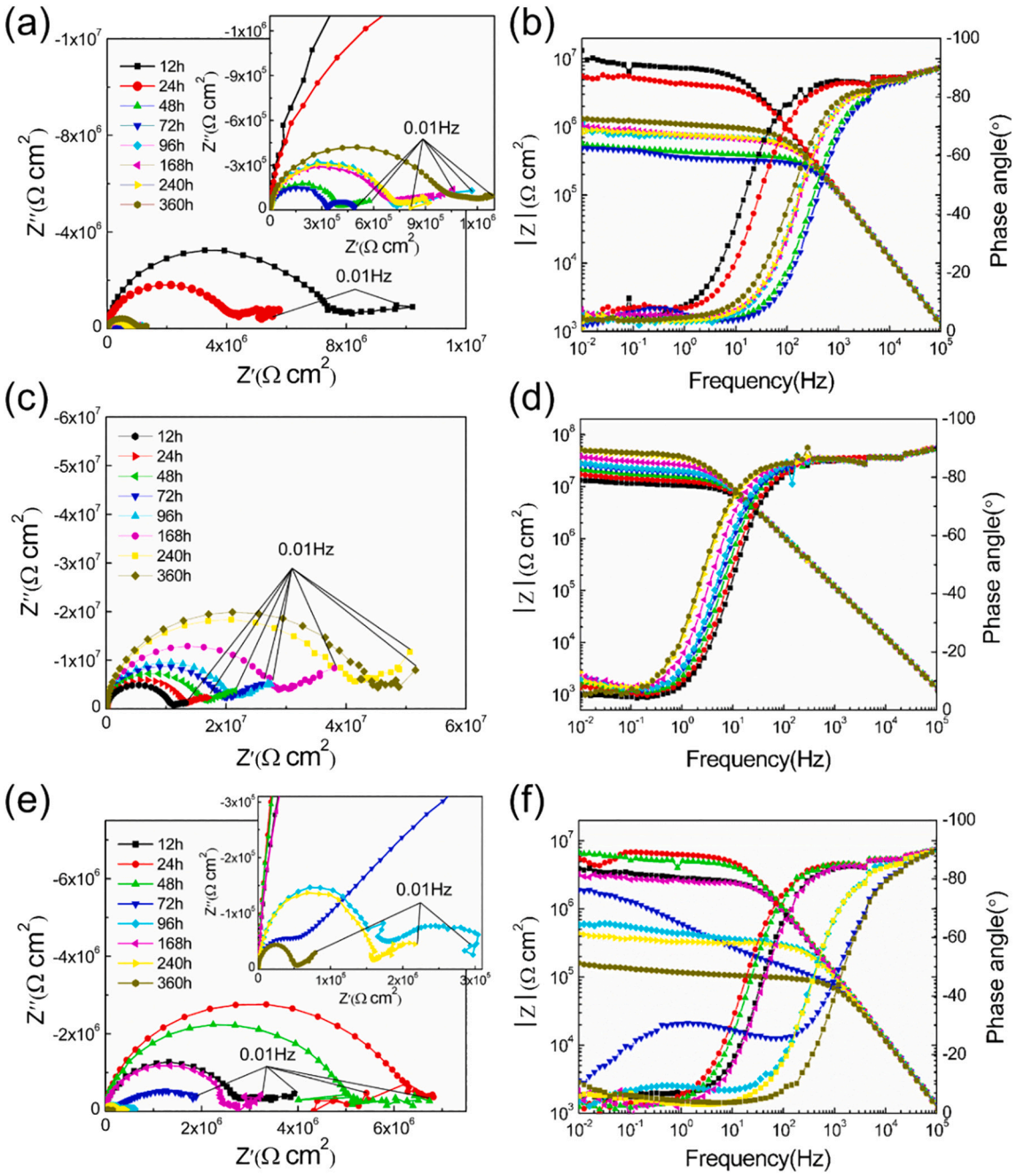

Fig. 11. Nyquist and Bode diagram of EIS measurements immersed in 3.5 wt% NaCl solution: (a)–(b) UI, (c)–(d) UIB-3, (e)–(f) UIS.

in the frequency range of 10^{-2} to 10 Hz. After immersing for 72 h, two time constants appear, indicating that the electrolyte reached the coating-steel interface, semicircles at high frequency correspond to coating properties while those at low frequency contain information related to reactions at the coating–metal interface [57] . For the UIB-3 coating system (Fig. 11(c) and (d)), the impedance modulus in low frequency (10^{-2} to 1 Hz) increases slowly during immersing process for 360 h and no corrosion reaction was observed. UIS coating system exhibited the worst corrosion protection ability as indicated by the rapid decrease of the impedance modulus in low frequency region (10^{-2} to 10 Hz) with immersion time. After immersion for 72 h, obvious corrosion reaction was found because two time constants were obtained in EIS [58–59]. Above all, the UIB-3 coating system demonstrated the best corrosion protection ability related to the addition of SiO_2@BTA. Fig. 12 shows the surface appearance of coated steel with defect after 1 day, 5 days and 15 days of immersion. Corrosion evolved rapidly in and from the coating defect of the UI covered steel due to its limited intrinsic self-healing properties. The accumulation of corrosion products in and below the UI layer even further prevented mobility of the UI polymer network across the coating defect. Compared with UI, UIB-3 which was loaded with 5 wt% SiO_2@BTA demonstrated a better corrosion protective effect upon application and exposure of the coating defect. To study the effect of adding SiO_2 on corrosion protection performance upon mechanical damage, we tested UIS with 5 wt% SiO_2 but no BTA as a comparative experiment. The results showed a high degree of corrosion attack within 5 days of exposure as shown in Fig. 12(c).

The mechanism of the enhanced corrosion protective ability upon mechanical damage was shown in Fig. 13. In this work, after addition of SiO_2@BTA, the materials exhibited faster self-healing process and enhanced corrosion protective performance at the same time compared

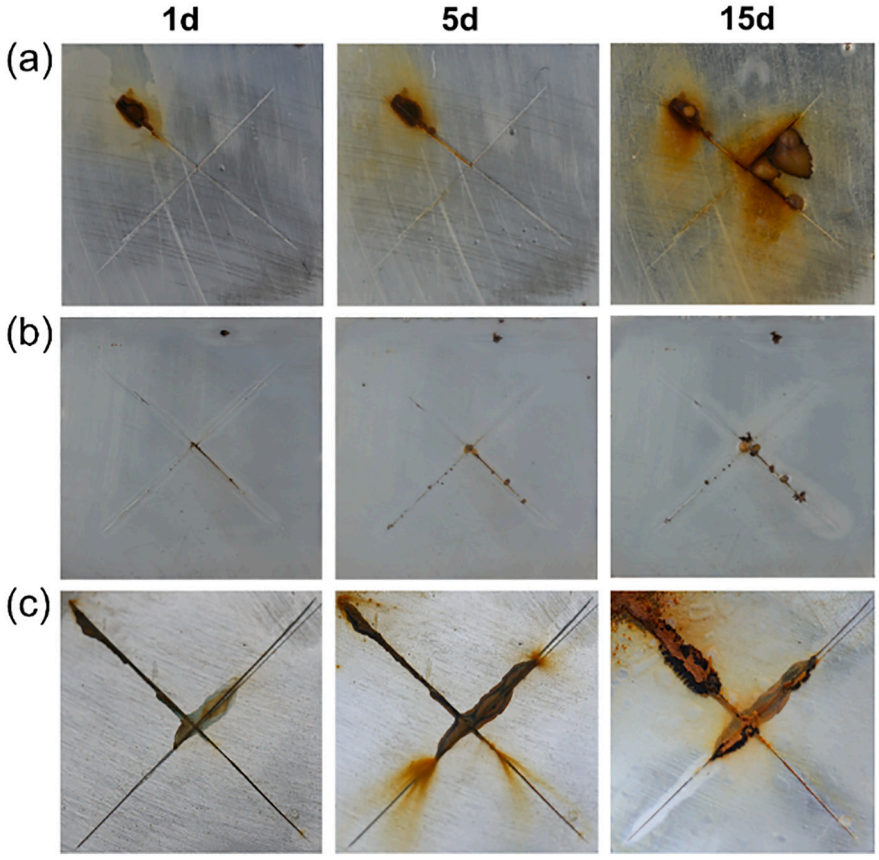

Fig. 12. Corrosion tests by immersion of the reference, SiO_2@BTA-loaded and SiO_2-loaded UI materials in 3.5% NaCl aqueous solution: (a) UI, (b) UIB-3, (c) UIS.

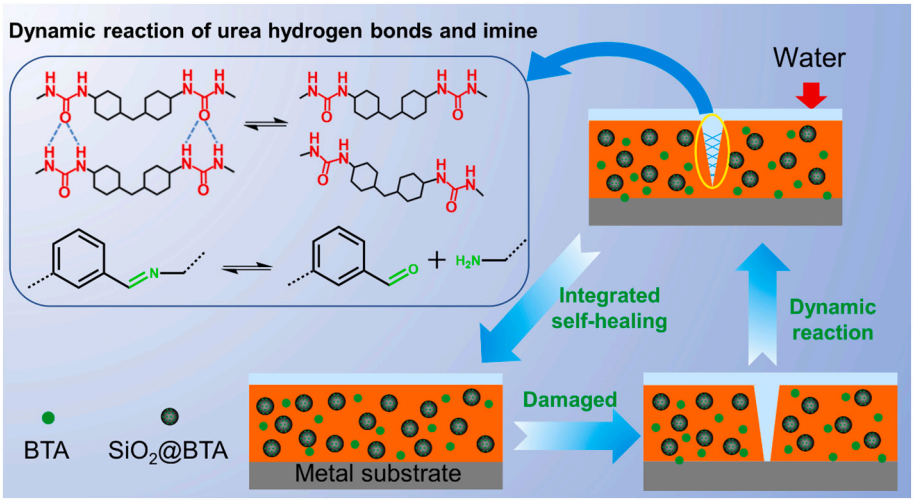

Fig. 13. Corrosion protective and self-healing mechanism of SiO_2@BTA loaded UI matrices in 3.5% NaCl aqueous solution.

with UI and UIS coatings. So it is reasonable to attribute the enhanced corrosion protection to the acceleration of self-healing process or interface mechanics. As the scratch was narrow, so some areas of the fracture interface can be re-contacted through restoration of the elastic strain. These contacted areas made it possible for the interspersed diffusion of polymer chain on the interface. Furthermore, the reversible reactions of urea hydrogen bonds and imine resulted in a substantial self-healing. Meanwhile, the contact and healed areas can spread around the interface through polymer chain diffusion and finally the barriers for corrosion protection were rebuilt to prevent passage of corrosive media.

In this process, the speed at which the corrosion barrier is rebuilt plays a decisive role. UIB-3 coating exhibited faster self-healing process compared with UI and UIS coatings, so corrosion barriers of UIB-3 can be rebuilt faster, in other words, the self-healing process occurred much faster than did the corrosion for this narrow scratch. For UI and UIS with low polymer chain activities and poor self-healing properties, it is the opposite condition that corrosion occurred before the corrosion barriers were rebuilt. There are some other researches supported similar results [60–61]. In addition, BTA releasing may also be directly beneficial to improve corrosion resistance of carbon steel upon mechanical scratch in

view of its significant corrosion inhibition performance [36], so in future research, we will implement strategies to control the release of BTA and increase the load efficiency of BTA to achieve better self-healing and corrosion protection effect.

4. Conclusion

In summary, an optimized self-healing composite coating was obtained by adding benzotriazole-loaded mesoporous SiO_2 nanoparticles to a dynamic network matrix cross-linked by urea hydrogen bonds and imine. The reversible cross-linked PDMS matrix achieved substantial and fast healing of the material integrity upon damage. BTA leaching tests demonstrated a longer release profile during the coating service life and corrosion tests in a 3.5 wt% NaCl aqueous solution indicated that the SiO_2@BTA modified PDMS coating shows an enhanced corrosion protection of carbon steel upon coating damage. The strength at failure increased to about 5.5 MPa for a BTA-loaded silica concentration of 5 wt %, which was three to four times higher than that of the unmodified reference UI matrix (~1.5 MPa for UI). Meanwhile, the self-healing efficiency increased from ~59% (reference UI) to ~90% (5 wt% BTA-loaded silica in UI matrix) for 24 h healing at room temperature. In the self-healing process, BTA played a vital role by forming hydrogen bonds with urea groups, which decreased the energy barrier in the reversible association-dissociation reaction of urea hydrogen bonds and active originally inert hydrogen bonds in hard segments. The increased mechanical strength results from the reinforcement of SiO_2 nanoparticles. This indicates that we found a promising material development strategy to minimize the commonly observed intrinsic conflict between high mechanical polymer strength and active polymer chain diffusion.

CRediT authorship contribution statement

Guangmeng Chen: Conceptualization, Data Curation, Writing - Original Draft. **Shifeng Wen**: Methodology, Writing - Review & Editing. **Jincheng Ma**: Formal analysis, Visualization. **Zhiyong Sun**: Supervision, Validation. **Cunguo Lin**: Investigation, Resources. **Zhufeng Yue**: Funding acquisition, Project administration. **J.M.C. Mol**: Review, Editing. **Ming Liu**: Formal analysis, Editing.

Declaration of competing interest

The authors declare that they have no known competing financial interests or personal relationships that could have appeared to influence the work reported in this paper.

Acknowledgements

The authors gratefully acknowledge the support for this work from the National Natural Science Foundation of China (No. 51872237, 12072273), Natural Science Basic Research Plan in Shaanxi Province of China (No. 2017JM5098), Provincial Natural Science Foundation of Shaanxi (No. 2018JM5032).

Appendix A. Supplementary data

The following files are available free of charge:

Particle size obtained by DLS (Fig. S1), SEM images (Fig. S2, S3), reaction scheme (Fig. S4, S7), FT-IR spectra (Fig. S5), stress relaxation curves (Fig. S6), DSC and XRD results (Fig. S8), scratch healing process of PU (Fig. S9), ultraviolet absorption spectrum (Fig. S10), stress-strain curves of UIB-0 after immersed in water (Fig. S11), scratch width measured by optical microscope (Fig. S12).

References

[1] Z. Chen, Y.C. Sun, J. Wang, H.J. Qi, T. Wang, H.E. Naguib, Flexible, reconfigurable, and self-healing tpu/vitrimer polymer blend with copolymerization triggered by bond exchange reaction, ACS Appl. Mater. Interfaces 12 (2020) 8740–8750.
[2] J. Chen, J. Liu, T. Thundat, H. Zeng, Polypyrrole-doped conductive supramolecular elastomer with stretchability, rapid self-healing, and adhesive property for flexible electronic sensors, ACS Appl. Mater. Interfaces 11 (2019) 18720–18729.
[3] M. Liu, Z. Wang, P. Liu, Z. Wang, H. Yao, X. Yao, Supramolecular silicone coating capable of strong substrate bonding, readily damage healing, and easy oil sliding, Sci. Adv. 5 (2019) eaaw5643.
[4] H. Chen, J. Cheng, L. Ran, K. Yu, B. Lu, G. Lan, F. Dai, F. Lu, An injectable self-healing hydrogel with adhesive and antibacterial properties effectively promotes wound healing, Carbohydr, Polym. 201 (2018) 522–531.
[5] S. Hafeez, H.W. Ooi, F.L.C. Morgan, C. Mota, M. Dettin, C. Van Blitterswijk, L. Moroni, M.B. Baker, Viscoelastic oxidized alginates with reversible imine type crosslinks: self-healing, injectable, and bioprintable hydrogels, Gels 4 (2018) 85.
[6] Y. Xu, Y. Li, Q. Chen, L. Fu, L. Tao, Y. Wei, Injectable and self-healing chitosan hydrogel based on imine bonds: design and therapeutic applications, Int. J. Mol. Sci. 19 (2018) 2198.
[7] Z. Wei, S. Gerecht, A self-healing hydrogel as an injectable instructive carrier for cellular morphogenesis, Biomaterials 185 (2018) 86–96.
[8] X. Wang, Y. Li, Y. Qian, H. Qi, J. Li, J. Sun, Mechanically robust atomic oxygen-resistant coatings capable of autonomously healing damage in low earth orbit space environment, Adv, Mater. 30 (2018), 1803854.
[9] F. Zhang, P. Ju, M. Pan, D. Zhang, Y. Huang, G. Li, X. Li, Self-healing mechanisms in smart protective coatings: a review, Corros, Sci. 144 (2018) 74–88.
[10] S. Wang, M.W. Urban, Self-healing polymers, Nat. Rev. Mater. 5 (2020) 562–583.
[11] A.A. Nazeer, M. Madkour, Potential use of smart coatings for corrosion protection of metals and alloys: a review, J. Mol. Liq. 253 (2018) 11–22.
[12] Y. Lai, X. Kuang, P. Zhu, M. Huang, X. Dong, D. Wang, Colorless, transparent, robust, and fast scratch-self-healing elastomers via a phase-locked dynamic bonds design, Adv, Mater. 30 (2018), 1802556.
[13] S.M. Kim, H. Jeon, S.H. Shin, S.A. Park, J. Jegal, S.Y. Hwang, D.X. Oh, J. Park, Superior toughness and fast self-healing at room temperature engineered by transparent elastomers, Adv, Mater. 30 (2018), 1705145.
[14] Y. Song, Y. Liu, T. Qi, G.L. Li, Towards dynamic but supertough healable polymers through biomimetic hierarchical hydrogen-bonding interactions, Angew, Chem., Int. Ed. 57 (2018) 13838–13842.
[15] Q. Zhang, S. Niu, L. Wang, J. Lopez, S. Chen, Y. Cai, R. Du, Y. Liu, J. C. Lai, L. Liu, C. H. Li, X. Yan, C. Liu, J. B. Tok, X. Jia, Z. Bao, An elastic autonomous self-healing capacitive sensor based on a dynamic dual crosslinked chemical system, Adv. Mater. 30 (2018) 1801435.
[16] F. Herbst, D. Doehler, P. Michael, W.H. Binder, Self-healing polymers via supramolecular forces, Macromol, Rapid Commun. 34 (2013) 203–220.
[17] Z. Mirzakhanzadeh, A. Kosari, M.H. Moayed, R. Naderi, P. Taheri, J.M.C. Mol, Enhanced corrosion protection of mild steel by the synergetic effect of zinc aluminum polyphosphate and 2-mercaptobenzimidazole inhibitors incorporated in epoxy-polyamide coatings, Corros, Sci. 138 (2018) 372–379.
[18] M. Tonelli, P. Baglioni, F. Ridi, Halloysite nanotubes as nano-carriers of corrosion inhibitors in cement formulations, Materials 13 (2020).
[19] I.A. Kartsonakis, A.C. Balaskas, E.P. Koumoulos, C.A. Charitidis, G. Kordas, Incorporation of ceramic nanocontainers into epoxy coatings for the corrosion protection of hot dip galvanized steel, Corros, Sci. 57 (2012) 30–41.
[20] S.V. Lamaka, M.L. Zheludkevich, K.A. Yasakau, R. Serra, S.K. Poznyak, M.G. S. Ferreira, Nanoporous titania interlayer as reservoir of corrosion inhibitors for coatings with self-healing ability, Prog, Org. Coat. 58 (2007) 127–135.
[21] Y. Morozov, L.M. Calado, R.A. Shakoor, R. Raj, R. Kahraman, M.G. Taryba, M. F. Montemor, Epoxy coatings modified with a new cerium phosphate inhibitor for smart corrosion protection of steel, Corros, Sci. 159 (2019), 108128.
[22] S. H. Cho, H. M. Andersson, S. R. White, N. R. Sottos, P. V. Braun, Polydimethylsiloxane-based self-healing materials, Adv. Mater. 18 (2006) 997–1000.
[23] S.A. Haddadi, S.A.A. Ramazani, M. Mahdavian, P. Taheri, J.M.C. Mol, Fabrication and characterization of graphene-based carbon hollow spheres for encapsulation of organic corrosion inhibitors, Chem. Eng. J. 352 (2018) 909–922.
[24] N. Pirhady Tavandashti, M. Ghorbani, A. Shojaei, J.M.C. Mol, H. Terryn, K. Baert, Y. Gonzalez-Garcia, Inhibitor-loaded conducting polymer capsules for active corrosion protection of coating defects, Corros, Sci. 112 (2016) 138–149.
[25] S. A. Haddadi, A. Ramazani S. A, M. Mahdavian, P. Taheri, J. M. C. Mol, Mechanical and corrosion protection properties of a smart composite epoxy coating with dual-encapsulated epoxy/polyamine in carbon nanospheres, Ind. Eng. Chem. Res. 58 (2019) 3033–3046.
[26] F. Maia, J. Tedim, A.D. Lisenkov, A.N. Salak, M.L. Zheludkevich, M.G. Ferreira, Silica nanocontainers for active corrosion protection, Nanoscale 4 (2012) 1287–1298.
[27] A. Phanasgaonkar, V.S. Raja, Influence of curing temperature, silica nanoparticles-and cerium on surface morphology and corrosion behaviour of hybrid silane coatings on mild steel, Surf, Coat. Technol. 203 (2009) 2260–2271.
[28] T. Chen, R. Chen, Z. Jin, J. Liu, Engineering hollow mesoporous silica nanocontainers with molecular switches for continuous self-healing anticorrosion coating, J. Mater. Chem. A 3 (2015) 9510–9516.
[29] J.-B. Xu, Y.-Q. Cao, L. Fang, J.-M. Hu, A one-step preparation of inhibitor-loaded silica nanocontainers for self-healing coatings, Corros, Sci. 140 (2018) 349–362.

[30] J. Wen, J. Lei, J. Chen, L. Liu, X. Zhang, L. Li, Polyethylenimine wrapped mesoporous silica loaded benzotriazole with high ph-sensitivity for assembling self-healing anti-corrosive coatings, Mater. Chem. Phys. 253 (2020), 123425.
[31] O. Geuli, D. Mandler, The synergistic effect of benzotriazole and trimethylsiloxysilicate towards corrosion protection of printed cu-based electronics, Corros, Sci. 143 (2018) 329–336.
[32] M. Finšgar, I. Milošev, Inhibition of copper corrosion by 1,2,3-benzotriazole: a review, Corros, Sci. 52 (2010) 2737–2749.
[33] M. Finšgar, I. Milošev, Corrosion study of copper in the presence of benzotriazole and its hydroxy derivative, Mater. Corros. 62 (2011) 956–966.
[34] S. Wan, C.-H. Miao, R.-M. Wang, Z.-F. Zhang, Z.-H. Dong, Enhanced corrosion resistance of copper by synergetic effects of silica and bta codoped in polypyrrole film, Prog, Org. Coat. 129 (2019) 187–198.
[35] Y. Hao, Y. Zhao, X. Yang, B. Hu, S. Ye, L. Song, R. Li, Self-healing epoxy coating loaded with phytic acid doped polyaniline nanofibers impregnated with benzotriazole for q235 carbon steel, Corros, Sci. 151 (2019) 175–189.
[36] Y. Hao, Y. Zhao, B. Li, L. Song, Z. Guo, Self-healing effect of graphene@pani loaded with benzotriazole for carbon steel, Corros, Sci. 163 (2020), 108246.
[37] S.-H. Lee, S.-R. Shin, D.-S. Lee, Self-healing of cross-linked pu via dual-dynamic covalent bonds of a schiff base from cystine and vanillin, Mater. Des. 172 (2019), 107774.
[38] Y. Chen, A.M. Kushner, G.A. Williams, Z. Guan, Multiphase design of autonomic self-healing thermoplastic elastomers, Nat. Chem. 4 (2012) 467–472.
[39] M. Liu, P. Liu, G. Lu, Z. Xu, X. Yao, Multiphase-assembly of siloxane oligomers with improved mechanical strength and water-enhanced healing., Angew, Chem., Int. Ed. 57 (2018) 11242–11246.
[40] L. Zhang, Z. Liu, X. Wu, Q. Guan, S. Chen, L. Sun, Y. Guo, S. Wang, J. Song, E. M. Jeffries, C. He, F. L. Qing, X. Bao, Z. You, A highly efficient self-healing elastomer with unprecedented mechanical properties, Adv. Mater. 31 (2019) 1901402.
[41] Z. Liu, L. Zhang, Q. Guan, Y. Guo, J. Lou, D. Lei, S. Wang, S. Chen, L. Sun, H. Xuan, E.M. Jeffries, C. He, F.-L. Qing, Z. You, Biomimetic materials with multiple protective functionalities, Adv, Funct. Mater. 29 (2019), 1901058.
[42] G. Chen, S. Liu, Z. Sun, S. Wen, T. Feng, Z. Yue, Intrinsic self-healing organogels based on dynamic polymer network with self-regulated secretion of liquid for anti-icing, Prog, Org. Coat. 144 (2020), 105641.
[43] G. Chen, Y. Wang, J. Zheng, S. Wen, J. Zhang, L. Wang, J. Hou, C. Lin, Z. Yue, Designed preparation of silicone protective materials with controlled self-healing and toughness properties, Prog, Org. Coat. 140 (2020), 105483.
[44] D. Borisova, H. Moehwald, D.G. Shchukin, Mesoporous silica nanoparticles for active corrosion protection, ACS Nano 5 (2011) 1939–1946.
[45] D. Chen, F. Chen, X. Hu, H. Zhang, X. Yin, Y. Zhou, Thermal stability, mechanical and optical properties of novel addition cured pdms composites with nano-silica sol and mq silicone resin, Compos, Sci. Technol. 117 (2015) 307–314.
[46] N. Suzuki, S. Kiba, Y. Kamachi, N. Miyamoto, Y. Yamauchi, Unusual reinforcement of silicone rubber compounds containing mesoporous silica particles as inorganic fillers, Phys. Chem. Chem. Phys. 14 (2012) 3400–3407.
[47] E. Yilgor, T. Eynur, C. Kosak, S. Bilgin, I. Yilgor, O. Malay, Y. Menceloglu, G. L. Wilkes, Fumed silica filled poly(dimethylsiloxane-urea) segmented copolymers: preparation and properties, Polymer 52 (2011) 4189–4198.
[48] W.-C. Lin, W. Fan, A. Marcellan, D. Hourdet, C. Creton, Large strain and fracture properties of poly(dimethylacrylamide)/silica hybrid hydrogels, Macromolecules 43 (2010) 2554–2563.
[49] G. Hochleitner, E. Fursattel, R. Giesa, J. Groll, H.W. Schmidt, P.D. Dalton, Melt electrowriting of thermoplastic elastomers, Macromol. Rapid Commun. 39 (2018), 1800055.
[50] R.M. Versteegen, R.P. Sijbesma, E.W. Meijer, Synthesis and characterization of segmented copoly(ether urea)s with uniform hard segments, Macromolecules 38 (2005) 3176–3184.
[51] D. Yin, Enhancement of the anti-corrosion performance of composite epoxy coatings in presence of bta-loaded copper-based metal-organic frameworks, Int. J. Electrochem. Sci. (2019) 4240–4253.
[52] J.S. Laird, P. Visser, S. Ranade, A.E. Hughes, H. Terryn, J.M.C. Mol, Li leaching from lithium carbonate-primer: an emerging perspective of transport pathway development, Prog, Org. Coat. 134 (2019) 103–118.
[53] A.E. Hughes, A. Trinchi, F.F. Chen, Y.S. Yang, I.S. Cole, S. Sellaiyan, J. Carr, P. D. Lee, G.E. Thompson, T.Q. Xiao, Revelation of intertwining organic and inorganic fractal structures in polymer coatings, Adv, Mater. 26 (2014) 4504–4508.
[54] E. Javierre, Modeling self-healing mechanisms in coatings: approaches and perspectives, Coatings 9 (2019) 122.
[55] E. Javierre, S.J. García, J.M.C. Mol, F.J. Vermolen, C. Vuik, S. van der Zwaag, Tailoring the release of encapsulated corrosion inhibitors from damaged coatings: controlled release kinetics by overlapping diffusion fronts, Prog, Org. Coat. 75 (2012) 20–27.
[56] S.A. Furman, F.H. Scholes, A.E. Hughes, D. Lau, Chromate leaching from inhibited primers, Prog, Org. Coat. 56 (2006) 33–38.
[57] X. Yuan, Z.F. Yue, Z.Q. Liu, S.F. Wen, L. Li, T. Feng, Effect of siloxane-modified polyacrylate on water uptake and anticorrosion mechanism of silicone–epoxy coatings, J. Coat. Technol. Res. 13 (2015) 123–132.
[58] J.M. Hu, J.Q. Zhang, C.N. Cao, Determination of water uptake and diffusion of cl− ion in epoxy primer on aluminum alloys in nacl solution by electrochemical impedance spectroscopy, Prog, Org. Coat. 46 (2003) 273–279.
[59] X. Yuan, Z.F. Yue, X. Chen, S.F. Wen, L. Li, T. Feng, The protective and adhesion properties of silicone-epoxy hybrid coatings on 2024 al-alloy with a silane film as pretreatment, Corros, Sci. 104 (2016) 84–97.
[60] Y. Cui, S. Song, Y. Tang, Y. Chen, H. Yang, B. Yang, J. Huang, Decoupling the roles of the catechol content from those of glass transition temperature and dynamic mechanical modulus in determining self-healing and anti-corrosion of mussel-inspired polymers, Polymer 185 (2019), 121928.
[61] B. Zhang, P. Zhang, H. Zhang, C. Yan, Z. Zheng, B. Wu, Y. Yu, A transparent, highly stretchable, autonomous self-healing poly(dimethyl siloxane) elastomer, Macromol, Rapid Commun. 38 (2017), 1700110.